Dirac solitons in square binary waveguide lattices

Truong X. Tran,[1,2] Xuan N. Nguyen,[1] and Fabio Biancalana[2,3]
[1]*Department of Physics, Le Quy Don University, 236 Hoang Quoc Viet Street, 10000 Hanoi, Vietnam*
[2]*Max Planck Institute for the Science of Light, Günther-Scharowsky-Straße 1/Bau 24, 91058 Erlangen, Germany*
[3]*School of Engineering and Physical Sciences, Heriot-Watt University, EH14 4AS Edinburgh, United Kingdom*
(Received 11 December 2014; published 11 February 2015)

We study optical analogs of two-dimensional (2D) Dirac solitons in square binary waveguide lattices with two different topologies in the presence of Kerr nonlinearity. These 2D solitons turn out to be quite robust. We demonstrate that with the found 2D solitons, the coupled mode equations governing light dynamics in square binary waveguide lattices can be converted into the nonlinear relativistic 2D Dirac equation with the four-component bispinor. This paves the way for using binary waveguide lattices as a classical simulator of quantum nonlinear effects arising from the 2D Dirac equation, something that is thought to be impossible to achieve in conventional (i.e., linear) quantum field theory.

DOI: 10.1103/PhysRevA.91.023814 PACS number(s): 42.65.Tg, 42.65.Wi, 42.81.Qb, 42.81.Dp

I. INTRODUCTION

Waveguide arrays have been used intensively to simulate the evolution of a nonrelativistic quantum-mechanical particle in a periodic potential. Many fundamental phenomena in nonrelativistic classical and quantum mechanics such as Bloch oscillations [1,2], Zener tunneling [3,4], optical dynamical localization [5], and Anderson localization in disordered lattices [6] have been simulated both theoretically and experimentally with waveguide arrays. In recent studies it was shown that, rather surprisingly, most of nonlinear fiber optics features (such as resonant radiation and soliton self-wave-number shift) can also take place in specially excited arrays [7,8]. Recently, binary waveguide arrays (BWAs) have also been used to mimic relativistic phenomena typical of quantum field theory, such as Klein tunneling [9,10], the *Zitterbewegung* (trembling motion of a free Dirac electron) [11,12], and fermion pair production [13], which are all based on the properties of the Dirac equation [14]. Quite recently, the optical analog of relativistic one-dimensional (1D) Dirac solitons have been analytically found in BWAs [15], and proved to be extremely robust [16]. In [15] we have provided analytical expressions for the nonmoving gap solitons in BWAs. We have also shown their connection to Dirac solitons in a nonlinear extension of the relativistic 1D Dirac equation describing the dynamics of a freely moving relativistic particle. Similar soliton solutions have been found for the nonlinear 1D Dirac equation [17], but with a different and more complicated kind of nonlinearity, in the context of quantum field theory. The discrete gap solitons in BWAs in the *classical* context have been investigated both numerically [18–20] and experimentally [21]. Although there is currently no evidence for fundamental quantum nonlinearities, nonlinear versions of the Dirac equation have been studied for a long time. One of the earlier extensions was investigated by Heisenberg [22] in the context of field theory and was motivated by the question of mass. In the quantum-mechanical context, nonlinear Dirac equations have been used as effective theories in atomic, nuclear, and gravitational physics [23–26] and, more recently, in the study of ultracold atoms [27,28]. To this regard, BWAs can offer a unique platform to simulate nonlinear extensions of the Dirac equation when probed at high light intensities. One of these possibilities is to use BWAs as a classical simulator of the Dirac equation to mimic the two-body Dirac model, i.e., the Dirac equation for two interacting relativistic particles, which has attracted a lot of interest from researchers since the early days of quantum mechanics [29,30].

Usual two-dimensional (2D) solitons in square binary lattices and at interfaces between binary lattices and homogeneous lattices were experimentally observed in [31,32]. The agreement between numerical simulations and experimental data for 2D solitons shown in [31,32] is strikingly excellent. Motivated by our recent achievements in the investigation of the optical analog of the relativistic 1D Dirac solitons in BWAs, and also by the success in experimental observations of usual solitons in square binary lattices, in this work we study the formation and dynamics of relativistic 2D Dirac solitons in square binary waveguide lattices (BWLs) with two different topologies. This paves the way for using BWLs to simulate nonlinear extensions of the 2D Dirac equation, as well as other solitonic and nonsolitonic effects of nonlinear 2D Dirac equations.

II. COUPLED-MODE EQUATIONS IN SQUARE BINARY WAVEGUIDE LATTICES

In this work we explore two different classes of square BWLs as shown schematically in Fig. 1. In Fig. 1(a) we illustrate the topology of class 1 BWLs where waveguides with two different types labeled “A” and “B” are arranged in a fashion such that each of the vertical and horizontal arrays of the lattice represents one BWA consisting of an alternating sequence of two waveguide types A and B. For class 2 BWLs as shown in Fig. 1(b), only vertical arrays are BWAs, whereas each horizontal array consists of only one type of waveguide—either “A” or “B.” Note that two types of waveguides can be different in any way, such as their sizes, geometries, and materials. The most important requirement is that their propagation constants must be different.

Light propagation in class 1 BWLs with Kerr nonlinearity can be described, in the continuous-wave regime (cw), by the following dimensionless coupled-mode equations

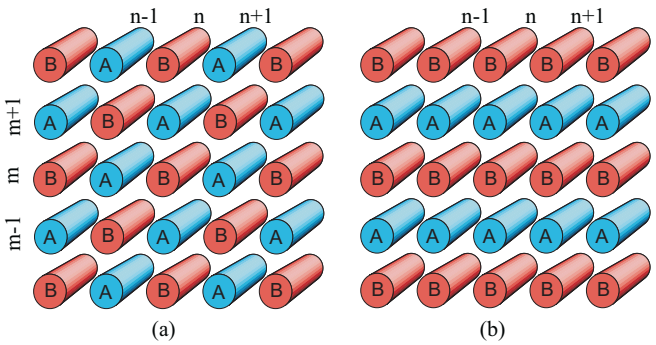

FIG. 1. (Color online) (a) Illustrative sketch of a square binary waveguide lattice of class 1 where each array (horizontal and vertical) consists of two alternating waveguides of types A and B. (b) Illustrative sketch of a square binary waveguide lattice of class 2 where each vertical array consists of two alternating waveguides of types A and B, whereas each horizontal array consists of just one type of waveguide (either A or B).

(CMEs):

$$i\frac{da_{m,n}(z)}{dz}+\kappa_1[(a_{m+1,n}+a_{m-1,n})+(a_{m,n+1}+a_{m,n-1})] +\kappa_2[(a_{m+1,n+1}+a_{m-1,n-1})+(a_{m+1,n-1}+a_{m-1,n+1})] -(-1)^{m+n}\sigma a_{m,n}+\gamma|a_{m,n}|^2a_{m,n}=0, \quad (1)$$

where $a_{m,n}$ is the electric field amplitude in the waveguide located in the mth row and nth column, z is the longitudinal spatial coordinate, 2σ is the propagation mismatch between two different types of waveguides, κ_1 and κ_2 are the coupling coefficients between neighboring waveguides of the lattice, and γ is the nonlinear coefficient of waveguides which is positive for self-focusing, but negative for self-defocusing media. The indices n and m run in the interval $[-N:N]$ and $[-M:M]$, respectively. For simplicity, here we suppose all waveguides have the same nonlinear coefficient, but even if these nonlinear coefficients are different (provided they are comparable), as shown in [15], then analytical soliton solutions of 1D Dirac solitons will remain unchanged, because one of the soliton components is much smaller than unity and the other component, and thus one can eliminate the nonlinear term associated with this weak soliton component. For the same reason, the difference in waveguide nonlinearity for 2D BWLs is also negligible in 2D Dirac soliton formation. In square lattices consisting of just one type of waveguide, the above CMEs without the term containing the propagation mismatch parameter σ in the linear regime were already reported in [33] [see Eq. (2.2) in [33]]. Now for square BWLs belonging to class 1 we just need to introduce this new term containing σ in Eq. (1) and a term taking into account the Kerr nonlinearity.

For square BWLs of class 2 shown in Fig. 1(b), light propagation in the cw regime is governed by the following CMEs:

$$i\frac{da_{m,n}(z)}{dz}+\kappa_1[(a_{m+1,n}+a_{m-1,n})+(a_{m,n+1}+a_{m,n-1})] +\kappa_2[(a_{m+1,n+1}+a_{m-1,n-1})+(a_{m+1,n-1}+a_{m-1,n+1})] -(-1)^{m}\sigma a_{m,n}+\gamma|a_{m,n}|^2a_{m,n}=0, \quad (2)$$

where the only difference with Eq (1) is in the term containing the propagation mismatch parameter σ [now we have the factor $(-1)^m$ in Eq. (2) instead of $(-1)^{m+n}$ in Eq. (1)]. Generally speaking, for square BWLs of class 2 there should be more than two coupling coefficients; for instance, the coupling coefficient κ_1^r between two neighboring identical waveguides in the same row [i.e., between the waveguide at the site (m,n) with waveguides at sites $(m,n+1)$ and $(m,n-1)$] can differ from the coupling coefficient κ_1^c between two neighboring different waveguides in the same column [i.e., between the waveguide at the site (m,n) with waveguides at sites $(m+1,n)$ and $(m-1,n)$]. However, for square lattices consisting of two types of waveguides which are not too different, the variation between κ_1^r and κ_1^c will be less than the one between them with κ_2, so in this work, for simplicity we will use just the coupling coefficient κ_1 and κ_2 as in Eq. (2). Equations (1) and (2) can be easily normalized such that the coupling coefficient $\kappa_1=1$ and the nonlinear coefficient $\gamma=1$. These values will be fixed further for these two coefficients. Due to the distances between neighboring waveguides, it is obvious that between two coupling coefficients exists the relationship $\kappa_1>\kappa_2$.

III. SOLITONS IN SQUARE BINARY WAVEGUIDE LATTICES OF CLASS 1

In this section we investigate the formation and dynamics of 2D solitons in square BWLs of class 1 with topology shown in Fig. 1(a). As mentioned above, the analytical 1D Dirac soliton solutions to the CMEs for 1D BWAs have been found as follows [15]:

$$\begin{bmatrix}\psi_{2n}(z)\\ \psi_{2n-1}(z)\end{bmatrix} =\begin{bmatrix} i^{2n}\frac{2\kappa_1}{n_0\sqrt{\sigma\gamma}}\operatorname{sech}\left(\frac{2n}{n_0}\right)e^{iz[(2\kappa_1^2/n_0^2\sigma)-\sigma]}\\ i^{2n}\frac{2\kappa_1^2}{n_0^2\sigma\sqrt{\sigma\gamma}}\operatorname{sech}\left(\frac{2n-1}{n_0}\right)\tanh\left(\frac{2n-1}{n_0}\right)e^{iz[(2\kappa_1^2/n_0^2\sigma)-\sigma]}\end{bmatrix}. \quad (3)$$

This analytical soliton solution in BWAs is a one-parameter family where one parameter such as soliton peak amplitude or width can be arbitrary, provided that the quasicontinuous limit is used, i.e., the soliton width is large enough (the beam width parameter $n_0\geqslant 3.5$; see [15] for more details). The Dirac soliton solution in the form of Eq. (3) is valid in the case when γ and σ are positive. However, with this solution one can easily construct other Dirac soliton solutions for any sign of each parameter γ and σ [15]. In what follows we use the following initial condition at the square BWL input for simulating Eq. (1):

$$a_{m,n}(0)=f\psi_m(0)\psi_n(0)/\psi_0(0), \quad (4)$$

where the peak amplitude parameter f will be varied to investigate the 2D solitons generation in square BWLs. The evolution of the beam is illustrated in Fig. 2(a) in the (m,n,z) space for the parameter $f=1.16$. Four frames in Fig. 2(a) at specific propagation distance $z=0$, 40, 60, and 80 are shown in contour plots in Figs. 2(b), 2(c), 2(d), and 2(e), respectively, in the (m,n) plane.

As shown in Fig. 2(a), at the initial stage the profile of the beam is adjusted, then after reaching the propagation distance $z\simeq 20$ some radiation is emitted from the beam, and then after

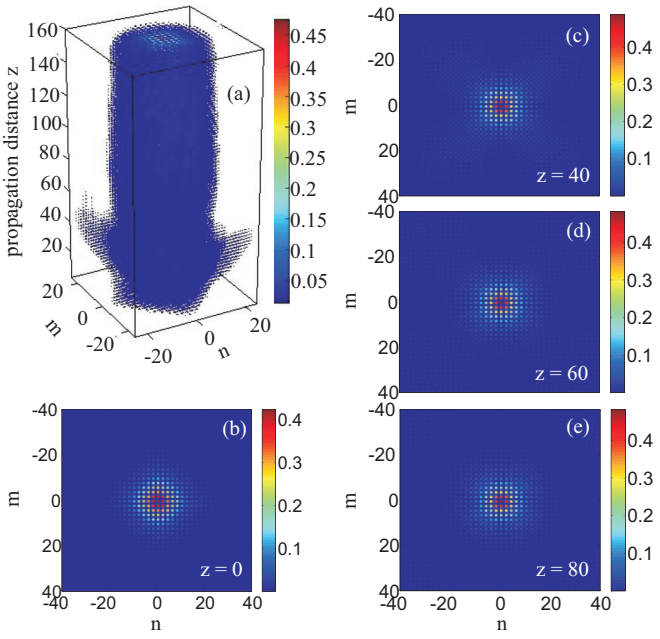

FIG. 2. (Color online) (a) Formation of a 2D soliton in the (m,n,z) space in square BWLs of class 1 when $\kappa_1 = 1$ and $\kappa_2 = 0.5$. (b)–(e) Contour plot of the beam at a specific frame with $z = 0$, 40, 60, and 80, respectively. Other parameters: $f = 1.16$, $\sigma = -1.2$, $\gamma = 1$, $n_0 = 5$, and $N = M = 60$.

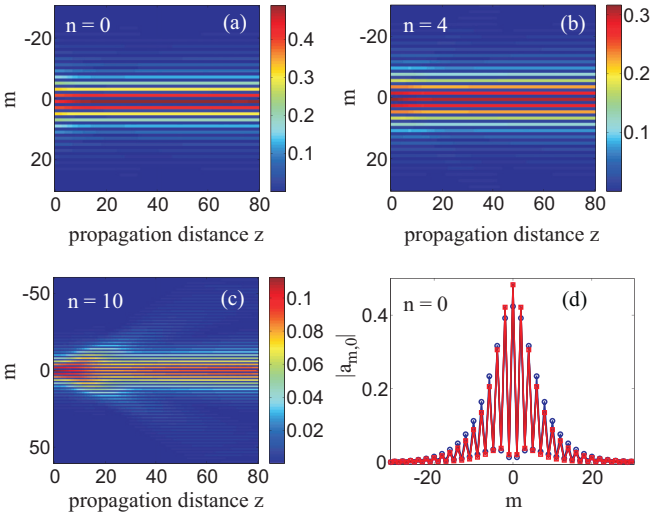

FIG. 3. (Color online) (a)–(c) Beam propagation along the z axis in the section containing the waveguide with index $n = 0$, 4, and 10, respectively, and parallel to the m axis. (d) The blue (red) curves with round (square) markers represent the input (output) signal in (a). The beam profile at the distance $z = 60$ is represented by the green curve in (d), but this curve is hardly visible because it is hidden by the red curve. All parameters are the same as in Fig. 2.

reaching the propagation distance $z \simeq 50$ the beam profile becomes very stable, and the beam now propagates without any significant distortion in profile and amplitude. As clearly shown in the contour plot in Fig. 2(b), the initial profile of the beam is reminiscent of a square, in particular in the periphery where amplitudes are weak. Note that weak features in four contour plots in Fig. 2 will be much more visible if one enlarges these contour plots, and due to limited resolution some weak features are invisible in the three-dimensional (3D) structure in Fig. 2(a), although they can be seen in 2D contour plots in Fig. 2. At the distance $z = 40$, as shown in Fig. 2(c), the radiation is generated and located in regions close to four corners of the contour plot in Fig. 2(c). However, the radiation in Fig. 2(c) still strongly overlaps with the central part of the beam. At the distance $z = 60$, as shown in Fig. 2(d), the radiation moves away from the central part of the beam toward four corners of the contour plot in Fig. 2(d), and the profile of the central part of the beam looks like a circle now. Finally, at the output frame when $z = 80$ the radiation now moves to tiny regions of four corners in Fig. 2(e), and is completely detached from the central part of the beam, thus with the formation of the central part of the beam we get a clean 2D soliton whose circlelike profile is well maintained during propagation. It is noteworthy mentioning that although the initial profile of the beam launched into the square BWL of class 1 is not exactly the one of a 2D soliton, during propagation the beam will nevertheless adjust its profile towards that of a 2D soliton. This feature shows that 2D solitons in BWLs of class 1 form spontaneously and are quite robust. To estimate real physical parameters of the calculated soliton we use typical parameters in waveguide arrays made of AlGaAs [2], where the coupling coefficient and nonlinear parameter in physical units $K_1 = 1240\ \mathrm{m}^{-1}$ and $\Gamma = 6.5\ \mathrm{m}^{-1}\,\mathrm{W}^{-1}$, respectively. In this case, the power scale will be $P_0 = K_1/\Gamma = 190.8$ W, thus the peak power of the soliton shown in Fig. 2 will be around 40.0 W and the length scale in the propagation direction will be $z_0 = 1/K_1 = 0.8$ mm. Instead of using cw beams, a common practice is to use short optical pulses with high peak power but wide enough that the dispersion effects are not important.

We now analyze three longitudinal sections of Fig. 2(a) along the z axis. The section containing the waveguide with index $n = 0$, 4, and 10 and parallel to the m axis is shown in the contour plots in Figs. 3(a), 3(b), and 3(c), respectively. The common feature of beam evolution in the first two contour plots in Figs. 3(a) and 3(b) is that at the beginning the beam slightly adjusts its profile, and then from a propagation distance $z \simeq 40$ the established profile of the 2D soliton is very stable. However, the beam profile in Fig. 3(c) undergoes significant changes: at first the beam broadens, then at the distance $z \simeq 20$ one can clearly see the radiation emitted away from the central part of the beam, and then after reaching the distance $z \simeq 60$ the central part of the beam profile almost does not change during propagation, whereas the radiation gets completely detached from the central part of the beam. The blue (red) curve with round (square) markers in Fig. 3(d) represents the input (output) in Fig. 3(a). The output red curve with square markers has a higher peak and smaller width as compared to the input blue curve with round markers. Actually, apart from the blue and red curves showing the input and output profiles in Fig. 3(d) we also plot the beam profile at the distance $z = 60$ with a green curve, but because at this distance the 2D soliton has been formed, its profile is well conserved and the intermediate green curve is completely hidden by the output red curve in Fig. 3(d).

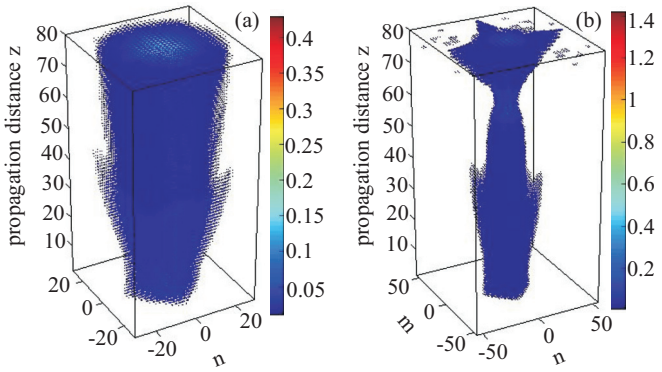

FIG. 4. (Color online) (a),(b) Evolution of beam in the (m,n,z) space when the peak amplitude parameter $f = 1.136$ and 1.170, respectively. All other parameters are the same as in Fig. 2.

In this section we illustrate the generation and formation of 2D solitons in square BWLs of class 1 with specific coupling coefficients $\kappa_1 = 1$ (fixed) and $\kappa_2 = 0.5$. However, our numerous simulations reveal that 2D solitons in square BWLs of class 1, which possess all main features of the 2D soliton shown in Figs. 2 and 3, can be generated with many different values of $\kappa_2 < \kappa_1$, including a special value $\kappa_2 = 0$. The latter case is important, because under this condition Eq. (1) can be converted into a 2D nonlinear relativistic Dirac equation as shown later in Sec. V.

In Figs. 2 and 3 we use the initial condition with the peak amplitude parameter $f = 1.16$ and, as a result, a 2D soliton is generated during propagation. If we now launch a beam into BWLs with lower initial peak amplitudes, it is reasonable to expect that in this case the diffraction-based broadening prevails over the nonlinearity-based focusing and the beam will spread out in space. Indeed, this is the case as shown in Fig. 4(a) with $f = 1.136$. On the contrary, if initial peak amplitudes are higher, then one can expect the focusing will prevail over the broadening. This is demonstrated in Fig. 4(b) with $f = 1.170$. After emitting the radiation at the distance $z \simeq 40$ the beam in Fig. 4(b) undergoes the compression, and after reaching the maximum compression at the distance $z \simeq 60$ the beam broadens quickly. Of course, the closer the initial peak amplitude to the value $f = 1.160$, the better the beam will conserve its shape during propagation as the 2D soliton shown in Figs. 2 and 3.

IV. SOLITONS IN SQUARE BINARY WAVEGUIDE LATTICES OF CLASS 2

In this section we investigate the formation and dynamics of 2D solitons in square BWLs of class 2 with topology shown in Fig. 1(b). In what follows we use the following initial condition at the square BWL input for simulating Eq. (2): $a_{m,n}(0) = f\psi_m(0)b_n/b_0$, where $b_n = (1/n_0)\mathrm{sech}(n/n_0)$, f is again the peak amplitude parameter. The evolution of the beam is illustrated in Fig. 5(a) in the (m,n,z) space for the parameter $f = 1.301$. Four frames in Fig. 5(a) at specific propagation distance $z = 0$, 60, 100, and 120 are shown in contour plots in Figs. 5(b), 5(c), 5(d), and 5(e), respectively, in the (m,n) plane.

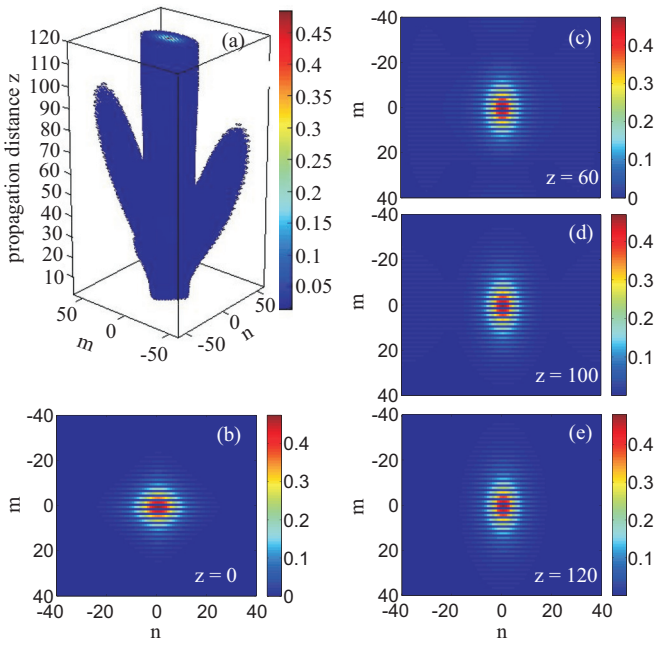

FIG. 5. (Color online) (a) Formation of a 2D soliton in the (m,n,z) space in square BWLs of class 2 when $\kappa_1 = 1$ and $\kappa_2 = 0.2$. (b)–(e) Contour plot of the beam at a specific frame with $z = 0$, 60, 100, and 120, respectively. Other parameters: $f = 1.301$, $\sigma = -1.2$, $\gamma = 1$, $n_0 = 5$, and $N = M = 150$.

As shown in Fig. 5(a), at the initial stage the profile of the beam is adjusted, then after reaching the propagation distance $z \simeq 20$ some radiation is emitted away from the beam, and then after reaching the propagation distance $z \simeq 80$ the central part of the beam profile becomes very stable propagating without any significant distortion in profile and amplitude. As clearly shown in the contour plot in Fig. 5(b), the initial profile of the beam is also reminiscent of a square consisting of stripes parallel to the n axis. Like in Fig. 2, weak features in four contour plots in Fig. 5 will be much more visible if one enlarges these contour plots, and due to limited resolution some weak features are invisible in the 3D structure in Fig. 5(a), although they can be seen in 2D contour plots in Fig. 5. At the distance $z = 60$, as shown in Fig. 5(c), the radiation is located close to four sides of the contour plot in Fig. 5(c). However, the radiation signal which is close to two sides parallel to the m axis is weaker than the one close to two sides parallel to the n axis. That is why one can only see the radiation signal close to two sides parallel to the n axis in the 3D structure in Fig. 5(a). The radiation in Fig. 5(c) still strongly overlaps with the central part of the beam. At the distance $z = 100$, as shown in Fig. 5(d), the radiation signal close to two sides parallel to the n axis is completely detached away from the central part of the beam whose profile looks like an oval now. Finally, at the output frame when $z = 120$ all the radiation now is completely detached from the central part of the beam and moves out completely from the frames used in Figs. 5(a) and 5(e). Note that the profile of the central part of the beam is well conserved in Figs. 5(d) and 5(e) [see also Fig. 5(a)], thus with the formation of the central part of the beam we get a clean 2D soliton whose oval-like profile with stripes

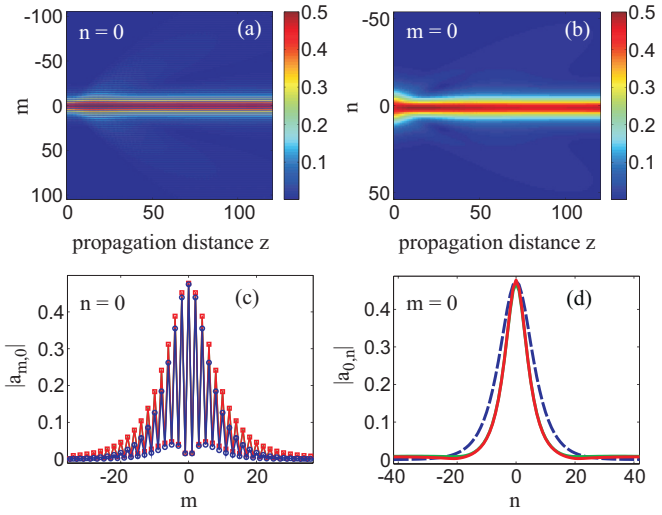

FIG. 6. (Color online) (a),(b) Beam propagation along the z axis in the section containing the waveguide with index $n = 0$ and $m = 0$, respectively. (c) The blue (red) curve with round (square) markers represents the input (output) signal in (a). (d) The dashed blue (solid red) curve represents the input (output) signal in (b). The beam profiles at the distance $z = 100$ are represented by green curves in (c) and (d), but these curves are hardly visible because they are hidden by the red curves.

parallel to the n axis is well maintained during propagation. It is noteworthy mentioning that although the initial profile of the beam launched into the square BWL of class 2 is not exactly the one of a 2D soliton for this kind of BWL, during propagation the beam will nevertheless adjust its profile towards that of a 2D soliton. This feature shows that 2D solitons in BWLs of class 2, like in BWLs of class 1, form spontaneously and are quite robust.

We now analyze two special sections of Fig. 5(a) along the z axis. The section containing the waveguide with index $n = 0$ and parallel to the m axis is shown in Fig. 6(a), whereas the section containing the waveguide with index $m = 0$ and parallel to the n axis is shown in Fig. 6(b). The common feature of beam evolution in Figs. 6(a) and 6(b) is that at the beginning the beam is slightly adjusted [broadened in Fig. 6(a) and compressed in Fig. 6(b)], and then from a propagation distance $z \simeq 50$ the established profiles of the 2D soliton in analyzed sections are very stable. The blue (red) curve with round (square) markers in Fig. 6(c) represents the input (output) signal in Fig. 6(a). Meanwhile, the dashed blue (solid red) curve in Fig. 6(d) represents the input (output) signal in Fig. 6(b). Actually, in Figs. 6(c) and 6(d) we also plot the corresponding beam profiles at the distance $z = 100$ by green curves; however, one almost cannot see this intermediate curve in Fig. 6(c), and can hardly see this green curve at the tails of signals shown in Fig. 6(d). This is because at this distance the 2D soliton has been established, thus these intermediates curves are almost hidden by the output curves. Note that the peak amplitudes of the input and output signals shown in Figs. 6(c) and 6(d) are almost constant, but their widths significantly change. Indeed, in Fig. 6(c) the input profile (which is the profile of a 1D Dirac soliton in BWAs) has a narrower width as compared to the output profile (which is the profile of an established 2D soliton in BWLs of class 2), whereas in Fig. 6(d) the input profile (which is the profile of the sech function representing the fundamental soliton of the nonlinear Schrödinger equation [34]) has a larger width as compared to the output profile (which is the profile of the established 2D soliton in BWLs of class 2). This feature is peculiar, because one can expect that for solitons, normally, the peak amplitude will increase (decrease) if the width gets narrower (broader) [see Fig. 3(d)].

V. TWO-DIMENSIONAL DIRAC SOLITONS

As mentioned in the Introduction, BWAs have been used to mimic phenomena in both nonrelativistic and relativistic quantum mechanics. In [15] we have shown that one can transform the nonlinear CMEs governing the light propagation in BWAs into the one-dimensional nonlinear relativistic Dirac equation (NRDE). In this section we show that one can also successfully convert Eq. (1) governing the light propagation in BWLs of class 1 into the two-dimensional NRDE. After setting $a_{2m,2n} = (-1)^{m+n}\Psi_1(m,n)$, $a_{2m-1,2n} = -i(-1)^{m+n}\Psi_2(m,n)$, $a_{2m,2n-1} = -i(-1)^{m+n}\Psi_3(m,n)$, and $a_{2m-1,2n-1} = -(-1)^{m+n}\Psi_4(m,n)$, and following the standard approach developed in [11,12], one can introduce the two continuous transverse coordinates $x \leftrightarrow m$, $y \leftrightarrow n$, time coordinate $t \leftrightarrow z$, and the four-component bispinor $\Psi(x,y,t) = (\Psi_1,\Psi_2,\Psi_3,\Psi_4)^T$ which satisfies the following nonlinear equation:

$$i\partial_t\Psi = -i\kappa_1(\alpha\partial_x\Psi + \rho\partial_y\Psi) + \kappa_2\delta\partial_{xy}^2\Psi + \sigma\beta\Psi - \gamma G, \quad (5)$$

where the nonlinear terms $G \equiv (|\Psi_1|^2\Psi_1,|\Psi_2|^2\Psi_2,|\Psi_3|^2\Psi_3,|\Psi_4|^2\Psi_4)^T$; α is a 4×4 matrix with all elements equal to zero, except $\alpha_{1,2} = \alpha_{2,1} = \alpha_{3,4} = \alpha_{4,3} = 1$; ρ is a 4×4 matrix with all elements equal to zero, except $\rho_{1,3} = \rho_{2,4} = \rho_{3,1} = \rho_{4,2} = 1$; δ is a 4×4 matrix with off-diagonal elements equal to unity, and all other elements equal to zero; and $\beta = \mathrm{diag}(1,-1,-1,1)$. If the coupling coefficient $\kappa_2 = 0$, then Eq. (5) has the same structure as the 2D NRDE describing the dynamics of a freely moving relativistic particle reported in [35] in the linear regime. As mentioned above, in the case of 1D BWAs, Eq. (5) is reduced to the 1D NRDE reported in [15]. Note that the nonlinearity that we have in Eq. (5) violates Lorentz invariance [36], and is similar to that of the Dirac equations in Bose-Einstein condensates [27]. Because the 2D soliton solutions of Eq. (1) exist and are stable as shown in Figs. 2 and 3, the 2D Dirac soliton solutions of Eq. (5) also exist and are stable. It is crucially important to emphasize that with the properties of the 2D solitons investigated in Sec. III, and with the above transformation rules connecting $a_{m,n}(z)$ to the four-component bispinor $\Psi(x,y,t)$, in the quasicontinuous limit, four components of the bispinor $\Psi(x,y,t)$ are smooth functions, and thus all derivatives in Eq. (5) make sense. In other conditions, it is not always possible to convert Eq. (1) into Eq. (5). This feature is also true for the case of 1D NRDE as already pointed out in [15]. To clarify this important point better, as an example, let us analyze the component Ψ_1 at the beginning

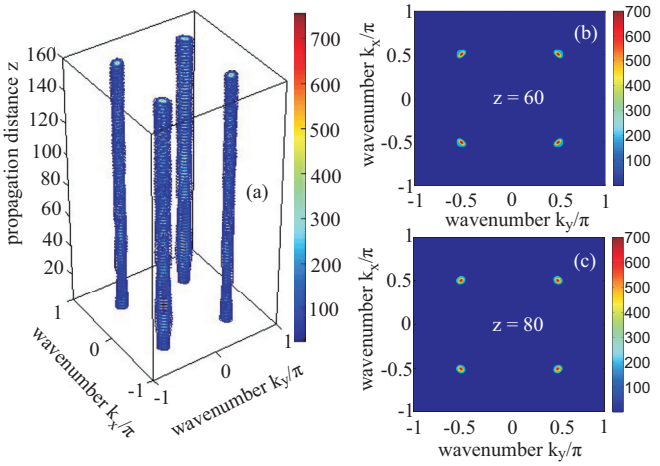

FIG. 7. (Color online) (a) Evolution of the spatial spectral of the 2D soliton in the (k_x,k_y,z) space in square BWLs of class 1. (b),(c) Contour plot of the spatial spectrum of the 2D soliton at a specific frame with $z = 60$ and 80, respectively. Parameters are the same as in Fig. 2.

(where $z = 0$):

$$\Psi_1(m,n) = \frac{a_{2m,2n}(0)}{(-1)^{m+n}} = \frac{1}{(-1)^{m+n}} \frac{f\psi_{2m}(0)\psi_{2n}(0)}{\psi_0(0)}$$
$$= \frac{i^{2(m+n)}}{(-1)^{m+n}} f \frac{2\kappa_1}{n_0\sqrt{\sigma\gamma}} \mathrm{sech}\left(\frac{2m}{n_0}\right)\mathrm{sech}\left(\frac{2n}{n_0}\right)$$
$$= f \frac{2\kappa_1}{n_0\sqrt{\sigma\gamma}} \mathrm{sech}\left(\frac{2m}{n_0}\right)\mathrm{sech}\left(\frac{2n}{n_0}\right). \quad (6)$$

Thus, in the quasicontinuous limit,

$$\Psi_1(m,n) \leftrightarrow \Psi_1(x,y) = f \frac{2\kappa_1}{n_0\sqrt{\sigma\gamma}} \mathrm{sech}\left(\frac{2x}{n_0}\right)\mathrm{sech}\left(\frac{2y}{n_0}\right), \quad (7)$$

and in this case, it is clear that all the derivatives $\partial_x\Psi_1, \partial_y\Psi_2$ and $\partial^2_{xy}\Psi_1$ in Eq. (5) exist. Analogously, one can easily confirm that all other derivatives of Ψ_2, Ψ_3, and Ψ_4 with respect to x and y also exist. Our numerical analysis also shows that for the soliton shown in Fig. 2 four components of $\Psi(x,y)$ are also smooth functions during propagation, which means that the derivatives in Eq. (5) exist not only for the beginning (where $z = t = 0$), but also for other values of z and t. Indeed, in Fig. 7(a) we show the spatial spectrum evolution of the 2D Dirac soliton illustrated in Fig. 2. The contour plot of this spatial spectrum at two specific frames with $z = 60$ and 80 is shown in Figs. 7(b) and 7(c), respectively. In Fig. 7, k_x and k_y are two components of the wave number in the x axis and y axis, respectively. As clearly shown in Fig. 7, k_x and k_y can only have values around $\pm\pi/2$ during propagation (see also Fig. 2 in [15]).

Note that due to the factor i^{2n} in Eq. (3), $a_{m,n}$ itself is not a smooth function. Indeed, as an example, where $z = 0$ the sign of $a_{m,n}$ changes from negative to positive and vice versa when m or n jumps to its closest value [whereas the sign of each component of $\Psi(m,n)$ stays the same except for the moments when functions $\tanh(2n-1)$ and $\tanh(2m-1)$ cross the abscissa]. Thus, unlike $\Psi(x,y)$ one cannot talk about the derivatives with respect to x and y for $a(x,y)$ in the quasicontinuous limit.

VI. CONCLUSIONS

In conclusion, we have demonstrated with accurate numerical simulations the generation and dynamics of 2D solitons in BWLs of classes 1 and 2. These 2D solitons are quite robust as they can be formed from the initial beams which are not the exact 2D solitons in BWLs. We have also shown their connection to 2D Dirac solitons in a nonlinear extension of the 2D relativistic Dirac equation describing the dynamics of a freely moving relativistic particle. Our results suggest that BWLs can be used as a classical simulator to investigate relativistic 2D Dirac solitons, enabling one to realize an experimentally accessible model system of quantum nonlinearities that have been so far a subject of speculation in the foundation of quantum field theories. The analysis of analog of quantum field theory effects as those described in this work is applicable to virtually any nonlinear discrete periodic system supporting solitons, either classical or quantum, therefore making our results very general and of relevance to different systems beyond optics, such as ultracold atoms in optical lattices and trapped ions where analogs of linear relativistic effects, such as *Zitterbewegung*, have been studied and observed [37–39].

ACKNOWLEDGMENTS

T.X.T. (Max Planck Partner Group) and F.B. (Max Planck Research Group) are supported by the German Max Planck Society for the Advancement of Science (MPG).

[1] T. Pertsch, P. Dannberg, W. Elflein, A. Bräuer, and F. Lederer, Phys. Rev. Lett. **83**, 4752 (1999).
[2] R. Morandotti, U. Peschel, J. S. Aitchison, H. S. Eisenberg, and Y. Silberberg, Phys. Rev. Lett. **83**, 4756 (1999).
[3] M. Ghulinyan, C. J. Oton, Z. Gaburro, L. Pavesi, C. Toninelli, and D. S. Wiersma, Phys. Rev. Lett. **94**, 127401 (2005).
[4] H. Trompeter, T. Pertsch, F. Lederer, D. Michaelis, U. Streppel, A. Bräuer, and U. Peschel, Phys. Rev. Lett. **96**, 023901 (2006).
[5] S. Longhi, M. Marangoni, M. Lobino, R. Ramponi, P. Laporta, E. Cianci, and V. Foglietti, Phys. Rev. Lett. **96**, 243901 (2006).
[6] Y. Lahini, A. Avidan, F. Pozzi, M. Sorel, R. Morandotti, D. N. Christodoulides, and Y. Silberberg, Phys. Rev. Lett. **100**, 013906 (2008).
[7] Tr. X. Tran and F. Biancalana, Phys. Rev. Lett. **110**, 113903 (2013).
[8] Tr. X. Tran and F. Biancalana, Opt. Express **21**, 17539 (2013).
[9] S. Longhi, Phys. Rev. B **81**, 075102 (2010).
[10] F. Dreisow, R. Keil, A. Tünnermann, S. Nolte, S. Longhi, and A. Szameit, Europhys. Lett. **97**, 10008 (2012).
[11] S. Longhi, Opt. Lett. **35**, 235 (2010).

[12] F. Dreisow, M. Heinrich, R. Keil, A. Tünnermann, S. Nolte, S. Longhi, and A. Szameit, Phys. Rev. Lett. **105**, 143902 (2010).
[13] S. Longhi, Appl. Phys. B **104**, 453 (2011).
[14] J. M. Zeuner, N. K. Efremidis, R. Keil, F. Dreisow, D. N. Christodoulides, A. Tünnermann, S. Nolte, and A. Szameit, Phys. Rev. Lett. **109**, 023602 (2012).
[15] Tr. X. Tran, S. Longhi, and F. Biancalana, Ann. Phys. (NY) **340**, 179 (2014).
[16] Tr. X. Tran, X. N. Nguyen, and D. C. Duong, J. Opt. Soc. Am. B **31**, 1132 (2014).
[17] Y. Nogami, F. M. Toyama, and Z. Zhao, J. Phys. A: Math. Gen. **28**, 1413 (1995).
[18] A. A. Sukhorukov and Y. S. Kivshar, Opt. Lett. **27**, 2112 (2002).
[19] A. A. Sukhorukov and Y. S. Kivshar, Opt. Lett. **28**, 2345 (2003).
[20] M. Conforti, C. De Angelis, and T. R. Akylas, Phys. Rev. A **83**, 043822 (2011).
[21] R. Morandotti, D. Mandelik, Y. Silberberg, J. S. Aitchison, M. Sorel, D. N. Christodoulides, A. A. Sukhorukov, and Y. S. Kivshar, Opt. Lett. **29**, 2890 (2004).
[22] W. Heisenberg, Rev. Mod. Phys. **29**, 269 (1957).
[23] D. C. Ionescu, J. Reinhardt, B. Müller, W. Greiner, and G. Soff, Phys. Rev. A **38**, 616 (1988).
[24] A. Zecca, Int. J. Theor. Phys. **41**, 421 (2002).
[25] M. J. Esteban and E. Sere, Discrete Contin. Dyn. Syst. **8**, 381 (2002).
[26] I. Bialynicki-Birula and J. Mycielski, Ann. Phys. (NY) **100**, 62 (1976).
[27] L. H. Haddad and L. D. Carr, Physica D **238**, 1413 (2009).
[28] L. H. Haddad and L. D. Carr, Europhys. Lett. **94**, 56002 (2011).
[29] N. Kemmer, Helv. Phys. Acta **10**, 47 (1937).
[30] E. Fermi and C. N. Yang, Phys. Rev. **76**, 1739 (1949).
[31] M. Heinrich, Y. V. Kartashov, L. P. R. Ramirez, A. Szameit, F. Dreisow, R. Keil, S. Nolte, A. Tünnermann, V. A. Vysloukh, and L. Torner, Opt. Lett. **34**, 3701 (2009).
[32] M. Heinrich, Y. V. Kartashov, L. P. R. Ramirez, A. Szameit, F. Dreisow, R. Keil, S. Nolte, A. Tünnermann, V. A. Vysloukh, and L. Torner, Phys. Rev. A **80**, 063832 (2009).
[33] F. Lederer, G. I. Stegeman, D. N. Christodoulides, G. Assanto, M. Segev, and Y. Silberberg, Phys. Rep. **463**, 1 (2008).
[34] G. P. Agrawal, *Nonlinear Fiber Optics*, 5th ed. (Academic, New York, 2013).
[35] P. A. M. Dirac, *The Principles of Quantum Mecchanics*, 4th ed. (Oxford University Press, New York, 1958).
[36] Nonlinear extensions of the Dirac equation that violate Lorentz invariance have been so far the subject of conjecture. See, for instance, R. R. Parwani, Ann. Phys. (N.Y.) **315**, 419 (2005); W. K. Ng and R. R. Parwani, SIGMA **5**, 023 (2009).
[37] L. Lamata, J. Leon, T. Schätz, and E. Solano, Phys. Rev. Lett. **98**, 253005 (2007).
[38] J. Y. Vaishnav and C. W. Clark, Phys. Rev. Lett. **100**, 153002 (2008).
[39] R. Gerritsma, G. Kirchmair, F. Zhringer, E. Solano, R. Blatt, and C. F. Roos, Nature (London) **463**, 68 (2010).